ELECTRICAL ENGINEERING AND ENERGY

OPEN ACCESS

Numerical Analysis and Simulation Approach of Copper Antimony Sulfide Based Thin Film Solar Cell with Dual Heterojunction

Hafizur Rahman Alve[1,3], Samia Azmol[2], and Mrinmoy Dey[3]

[1] Institute of Energy, University of Dhaka, Dhaka-1000, Bangladesh
[2] Dept. of Electrical and Electronic Engineering, Anwer Khan Modern University, Dhaka-1230, Bangladesh
[3] Dept. of Electrical and Electronic Engineering, Chittagong University of Engineering and Technology, Chattogram- 4349, Bangladesh

Submitted: 28 April 2026
Accepted : 02 June 2026
Online First: 10 June 2026

Corresponding author
Hafizur Rahman Alve,
alve8969@gmail.com

DOI:10.64470/elene.2026.32

Abstract: This paper presents a SCAPS-1D numerical investigation of a Copper Antimony Sulfide (CuSbS2)-based thin-film solar cell using a dual-heterojunction n-ZnSe/p-$CuSbS_2$/p+-BMO structure. The influence of ZnSe window-layer thickness and ferroelectric BSF materials including BFO, BTO and BMO was evaluated under AM1.5G illumination using literature-based material parameters. Under the adopted idealized simulation conditions, the optimized BMO-based structure produced Voc = 1.257 V, Jsc = 46.819 mA/cm², FF = 83.21% and PCE = 48.96%. Because this result is unusually high for a $CuSbS_2$-based thin-film device, it is interpreted as a numerical upper-limit case that requires further validation using complete optical, recombination and experimental device analysis.

Keywords $CuSbS_2$, Dual heterojunction, BSF, BMO, SCAPS-1D

1. Introduction

The PV equipment and materials may be utilized to transform solar energy into electrical energy. One single cell makes up a photovoltaic (PV) device. Photovoltaic (PV) cells are typically quite small and have a limited power output. Usually built of a variety of semiconductor materials, these phones have a thickness of less than four human hairs. To ensure that they can endure the environment for a long time, cells are encased in a combination of polymers and/or glass and placed between two layers of protection. To increase the amount of electricity that PV cells can generate, they are often joined to larger units called modules or boards. Modules can be combined with other modules or used alone to create arrays. Building a PV system from scratch ends with connecting one or more arrays to the local electricity grid. Because of its modular construction, photovoltaic (PV) systems may be created regardless of the demand for power.

Recently chalcopyrite semiconductors, such as $CuInSe_2$ (CIS), Cu_2ZnSnS_4 (CZTS) (Hafizur Rahman Alve, Mrinmoy Dey, et al. 2024), $CuSbS_2$ (Bhattacharjee et al. 2023), $CuSbSe_2$ (Hafizur Rahman Alve, Saiful Islam, et al. 2024), $CuGaSe_2$ (CGS) have drawn a lot of interest as promising and cutting-edge options for high-efficiency thin-film solar cell applications. For several reasons, researchers are looking at chalcostibite ($CuSbS_2$), a ternary I-V-VI2 chalcogenide (Asafu-Adjaye 2000), that is comparatively unknown, as a

possible photo-absorber (Koroneos, Spachos, and Moussiopoulos 2003). According to both theoretical and experimental estimates, $CuSbS_2$ has a straight band gap between 1.38 and 1.5 eV, making it perfect for absorber layers (Zhou et al. 2009). Around 10^4 cm^{-1} is its absorption coefficient at 1.5 eV (Rodriguez-Lazcano, Nair, and Nair 2001) band gap energy. $CuSbS_2$ has large dielectric constant, high hole mobility, and straightforward composition make it a potential absorber. Furthermore, the components that make up $CuSbS_2$ are widely available, reasonably priced, and non-toxic. $CuSbS_2$ is a non-toxic substitute for CZTS and CIGS since it is readily available. A variety of direct and indirect approaches, including physical and chemical procedures including thermal evaporation, co-sputtering, and also spin coating, have been used by researchers to synthesis copper antimony sulfide ($CuSbS_2$), yielding a range of characteristics.

The theoretical efficiency range of advanced heterojunction and multi-junction photovoltaic concepts can be high under idealized conditions(Martí and Luque 2015); however, such values cannot be directly applied to a single simulated $CuSbS_2$ absorber without careful consideration of optical absorption limits, recombination pathways, and device physics. Therefore, in this work the high simulated output of the proposed dual-heterojunction structure is interpreted as an upper-bound numerical result under the selected SCAPS-1D assumptions, not as an experimentally verified efficiency. Using ferroelectric materials as the back-surface layer, this study aims to evaluate whether a $CuSbS_2$-based device can be improved by rear-interface engineering and BSF-assisted carrier selectivity.

In order to determine the ideal window layer structure, we examine the performance of ZnSe window layers with different thicknesses. As a back surface field (BSF) layer, we used ferroelectric materials BTO, BFO, and BMO, and we assessed their performance according to thickness. For all these ferroelectric materials, we built dual-heterojunction solar cells, and the structure with the best power conversion efficiency (PCE) was n-ZnSe/p-$CuSbS_2$/p+-BMO.

2. Modeling and Simulation

The simulation was performed using SCAPS-1D and literature-based physical parameters. Numerical simulations were carried out under AM1.5G illumination with an incident power density of 100 mW/cm^2 at 300 K. Series and shunt resistances were included using the optimized values defined in the simulation setup. Bulk donor and acceptor defects were represented using Gaussian distributions, and interface-related defects were considered where applicable. In the original model, radiative recombination was not explicitly included; in the revised interpretation, this assumption is identified as a limitation because omission of radiative and other recombination pathways can lead to optimistic performance values. Therefore, the high PCE reported for the optimized structure should be understood as an idealized simulated upper-limit case that requires further validation using a more complete recombination model including radiative, Auger, and experimentally measured defect-assisted recombination parameters.

The simulated schematic design of the dual-heterojunction n-ZnSe/p-$CuSbS_2$/p+-BMO cell is shown in Figure 1. Nickel (Ni) acts as the back contact in this structure. Incoming light first passes through the ZnSe window layer and is mainly absorbed in the $CuSbS_2$ absorber, while the BMO rear layer is modeled as a p+-type BSF/hole-selective layer that modifies rear-interface energetics and may contribute to the simulated long-wavelength response only under the assumed material and defect parameters. $CuSbS_2$ has an ionization potential of 5.45 eV and an electron affinity of 4.05 eV, whereas ZnSe has an ionization potential of 6.79 eV(Sayeed and Khaled Rouf 2019). Because of this alignment, ZnSe can form the front p-n heterojunction with $CuSbS_2$. For consistency with Table 1 and the simulation input, BMO is treated with a bandgap of 1.2 eV and electron affinity of 3.75 eV, enabling a p-p+ rear heterojunction with $CuSbS_2$. This rear junction supports hole extraction and reduces rear-interface recombination in the idealized model.

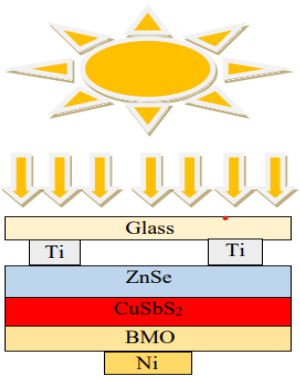

Figure 1 Proposed structure of $CuSbS_2$ solar cell.

Table 1 Electrical parameter of different layers for simulation in SCAPS

Material Properties	ZnSe (Saha et al. 2023)	$CuSbS_2$ (Bhattacharjee et al. 2023)	BMO (Branković et al. 2010)	BFO (Kumar, Saini, and Soam 2025)	BTO (Deng et al. 2026)
Thickness (μm)	0.05	0.8	0.2	0.2	0.2
Bandgap, Eg (eV)	2.7	1.45	1.2	2.26	1.67
Electron affinity (eV)	4.09	4.05	3.75	3.3	3.8
Dielectric permittivity	9.2	12	18.5	156	18.5
Nc (cm^3)	1.5×10^{18}	1.23×10^{20}	1.0×10^{16}	1.0×10^{16}	1.0×10^{16}
Nv (cm^3)	1.8×10^{19}	1.78×10^{20}	1.0×10^{17}	1.0×10^{17}	1.0×10^{17}
μe (cm^2/Vs)	50	4	180	200	100
μh (cm^2/Vs)	20	4	80	40	25
Na (cm^{-3})	0	5×10^{15}	7.5×10^{19}	7.5×10^{19}	7.5×10^{19}
Nd (cm^{-3})	1×1018	0	0	0	0
Type of defect	Acceptor	Donor	Neutral	Neutral	Neutral
Distribution	Gaussian	Gaussian	single	Single	Single
Nt [$eV^{-1}cm^{-3}$]	5.642×10^{13}	5.642×10^{13}	1×10^{14}	1×10^{14}	1×10^{14}
Reference Energy [eV]	1.350	0.650	0.6	0.6	0.6

3. Results and Discussion

3.1 Impact of Window Layers on Cell Performance

The ZnSe window layer generally has a range of ideal thicknesses that maximize solar cell conversion efficiency. A compromise between carrier collection and light transmission determines the ideal thickness. In order to successfully capture photogenerated carriers and ensure low carrier recombination as well as maximal current extraction, it should be thick enough. It should not, however, be very thick since this may prevent light from reaching the absorber layer, lowering the quantity of incoming light that can be absorbed and resulting in less photo-current production (Mahmood and Shah 2012). The conversion ability of a thin film solar cell may be altered by changing the thickness of the ZnSe window layer. This is essential for aiding effective carrier collection, lowering recombination losses, and improving the solar cell's overall efficiency (Ferekides et al. 2000).

Figure 2 shows the thickness variation of ZnSe window layer. The ZnSe window layer generally has a range of ideal thicknesses that maximize solar cell conversion efficiency. By varying thickness of ZnSe window layer from 0 to 200 nm, we observed almost constant value of Voc & FF. On the other hand, the value of Jsc increased. As a result, efficiency increased from 26.48 % to 29.47%. A compromise between carrier collection and light transmission determines the ideal thickness. To successfully capture photon generated carriers and ensure low carrier recombination as well as maximal current extraction, it should be thick enough. It should not, however, be very thick since this may prevent light from reaching the absorber layer, lowering the quantity of incoming light that can be absorbed and resulting in less photocurrent production.

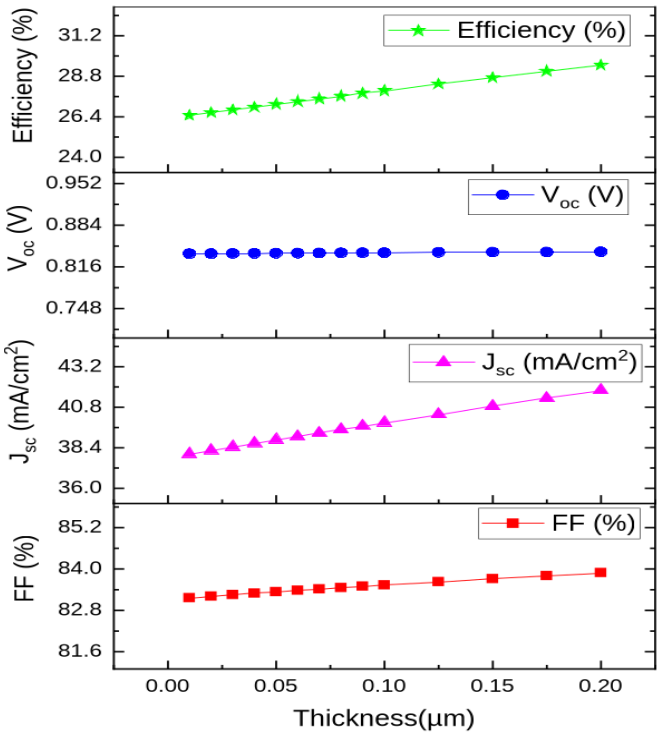

Figure 2 Thickness variation of ZnSe

3.2 Impact of BSF Layers on Cell Performance

At the solar cell's back surface, the BSF layer serves as a barrier to stop carrier recombination. By properly separating the photon generated electrons and holes in an area of high electric field, it decreases the likelihood of them being recombined and lengthens their lifespan. The BSF layer aids in maximizing the solar cell's total conversion efficiency by reducing carrier recombination (Borse, Chavhan, and Sharma 2007).

Through the creation of a stronger electric field close to the back surface, the BSF layer improves carrier collecting. This field directs the photon generated carriers towards the direction of contacts, enabling effective extraction. A greater photocurrent results from better carrier collection, which boosts the solar cell's overall performance. We use Bismuth manganite ($BiMnO_3$ or BMO) Ferroelectric materials as BSF layer. It's a complex oxide that has been investigated for a variety of applications, including its potential as a bottom Surface Field (BSF) coating in thin film solar cells. Although the use of BMO as a BSF coating in thin-film solar cells has not been studied as extensively as other materials, it has been utilized (Islam Sakib, Ahmed, and Dhar 2023).

3.3 Thickness Variation of BFO

The thickness of the Bismuth Ferrite (BFO) layer in a thin film solar cell can affect its performance, particularly conversion efficiency. The thickness of the BFO layer has an effect on the production and density of faults in the film. Thicker layers may be more susceptible to flaws like grain boundaries or fissures, which can impair carrier movement and raise recombination rates. Controlling the thickness can aid in the optimization of film quality and the reduction of defect-related losses (Kumar et al. 2025).

Figure 3 shows the comparison of thickness of BFO BSF layer from 0 to 400 nm, we observed almost constant value of Voc at 1.25V as well AS FF at 83.21% and also Jsc at 39.4 (mA/cm^2). As a result, the efficiency was almost same as 41.00% for all thickness.

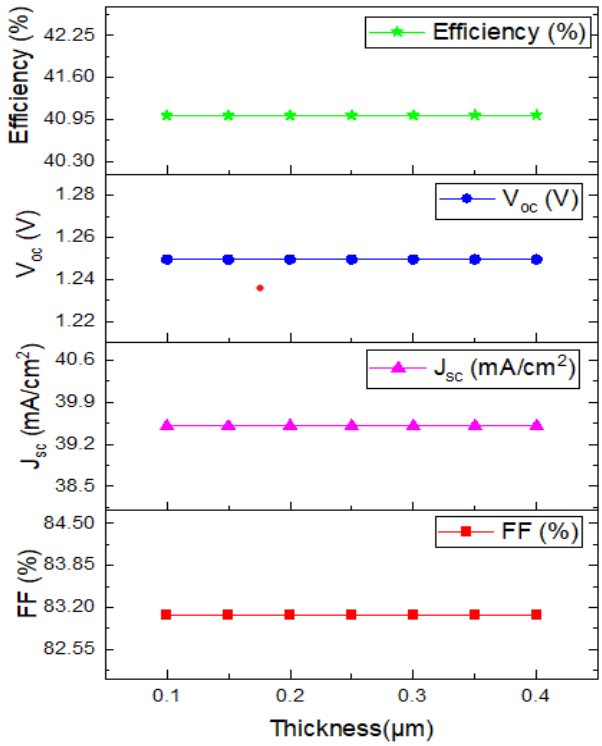

Figure 3 Thickness comparison of BFO BSF layer

3.4 Thickness Variation of BTO

The thickness of the Barium Titanate (BTO) layer in a thin film solar cell can affect device performance, particularly conversion efficiency. The effectiveness of the BTO layer to absorb light is affected by its thickness. Thicker BTO layers may absorb more photons, allowing the solar cell to absorb more light. Excessively thick layers, on the other hand, may impede light penetration into the underlying layers, lowering total photon absorption and potentially lowering conversion efficiency (Deng et al. 2026).

Figure 4 shows the thickness variation of the BTO BSF layer from 0 to 400 nm. After rechecking the reported values, the BTO-based device is described consistently with the comparative BSF table: Voc is approximately 1.249 V, Jsc is approximately 39.507 mA/cm², FF is approximately 83.08%, and PCE is approximately 41.01%. The response remains nearly unchanged with thickness within the investigated range, indicating that BTO provides a stable, but lower-performing BSF effect compared with BMO under the selected simulation parameters.

3.5 Thickness Variation of BMO

The performance of a thin film solar cell, particularly the conversion efficiency, can be affected by changing the thickness of the Bismuth Manganite (BMO) layer. The accumulation of photogenerated carriers is influenced by the BMO layer's thickness. Shorter carrier collection paths can be provided by thinner layers, lowering the chance of transporter recombination and increasing the effectiveness of charge collection. On the other side, larger layers can result in longer carrier transport pathways, raising the chance of carrier recombination and decreasing the effectiveness of charge collection (Islam Sakib et al. 2023).

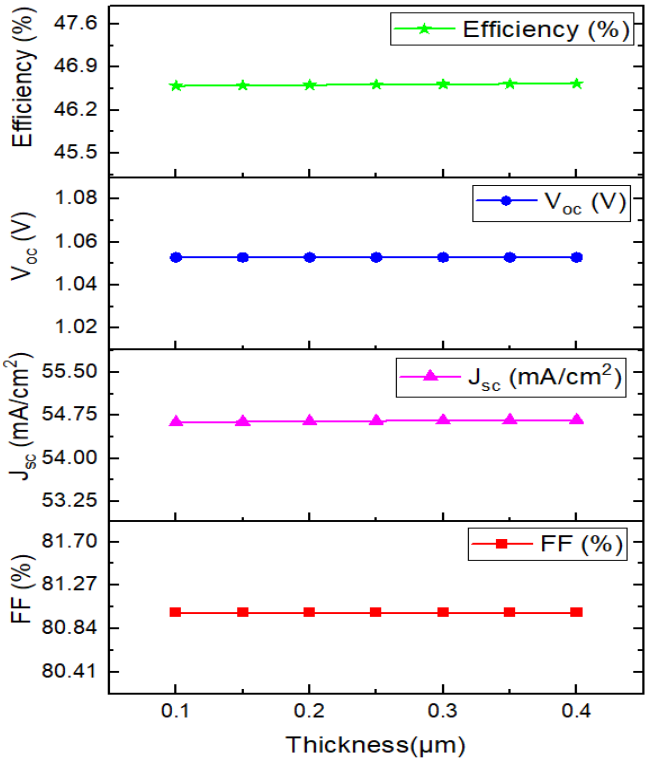

Figure 4 Thickness comparison of BTO BSF layer

Figure 5 shows the variation of BMO BSF-layer thickness from 0 to 200 nm. The values of Voc and FF remain nearly stable, while Jsc increases gradually with BMO thickness. As a result, the simulated efficiency increases from 45.58% to 48.96%. The 200 nm BMO thickness was selected as the optimized value in this numerical study. However, because the resulting PCE and Jsc are very high for a $CuSbS^2$-based device, the result is interpreted as an idealized upper-limit simulation outcome dependent on the assumed BMO parameters, rear-interface defect settings, and recombination model.

Table 2 Comparison of performance of different BSF layers

BSF Layer	Voc (V)	Jsc (mA/cm²)	FF (%)	PCE (%)
BFO	1.249	39.502	83.07	41.00
BTO	1.249	39.507	83.08	41.01
BMO	1.257	46.819	83.21	48.96

BMO possesses ferroelectric, magnetic, and multiferroic properties, which may support improved carrier separation and rear-interface selectivity in an idealized device model. In the revised interpretation, these properties are not treated as direct proof of experimentally confirmed up-conversion. Instead, the BMO layer is considered a rear BSF/hole-selective layer whose assumed bandgap, electron affinity, doping density, and defect-state distribution influence band alignment, carrier transport, and recombination. Any contribution from tail states or extended spectral response must therefore be regarded as model-dependent and require further validation by detailed optical modeling and experimental measurement.

Figure 6 illustrates the change in BMO doping concentration from 10^{10} cm^{-3} to 10^{21} cm^{-3}. The optimized BMO-based structure gives approximately Voc = 1.257 V, Jsc = 46.819 mA/cm^2, FF = 83.21%, and PCE = 48.96%. The previously reported FF inconsistency has been corrected. The simulation indicates that BMO gives the highest PCE among the investigated BSF layers, but this value should be interpreted cautiously because the model uses idealized rear-layer and recombination assumptions.

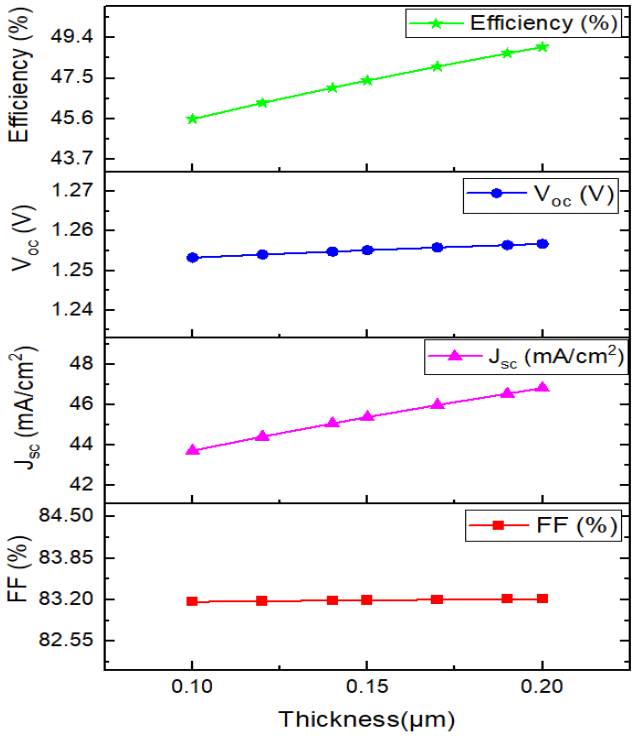

Figure 5 Thickness comparison of BMO BSF layer

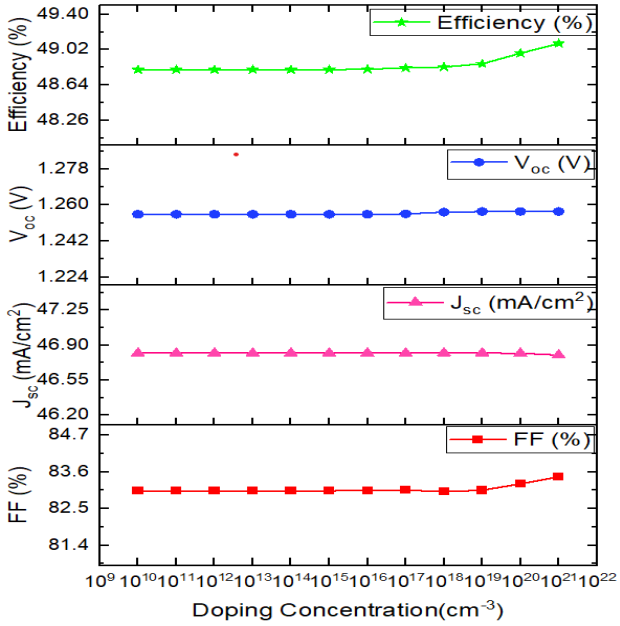

Figure 6 Doping Concentration Variation of BMO BSF layer.

3.6 Variation of Defect Density

The defect-density sweep was performed from 10^{11} cm^{-3} to 10^{19} cm^{-3} while maintaining the optimized layer thicknesses. The results show that the device output is relatively stable at lower defect densities but deteriorates when defect density becomes high, mainly because increased trap-assisted recombination reduces carrier lifetime and junction quality. For the optimized case, the representative parameters are Voc = 1.248 V, Jsc = 46.7 mA/cm^2, FF = 83.25%, and PCE close to 48.96%. Because the final performance is strongly affected by the selected defect density, experimentally measured defect parameters should be used in future validation studies.

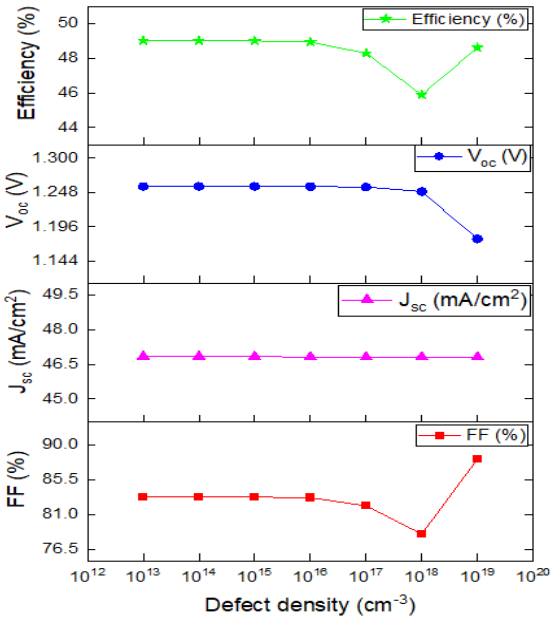

Figure 7 Variation of Defect Density for $CuSbS_2$ Solar Cell

3.7 Temperature variation's impact on $CuSbS_2$ solar cell

Changes in operating temperature affect all major cell parameters. As temperature increases, reverse saturation current generally rises (Javed 2022), which reduces the open-circuit voltage and weakens device stability. Figure 8 shows the temperature response of the proposed structure from 300 K to 500 K. The computed temperature coefficient is approximately -0.065%/°C under the adopted model. This value indicates favorable thermal behavior in the simulation, but it should be validated using a more complete recombination model because temperature sensitivity can be underestimated when radiative, Auger, and realistic defect-assisted recombination pathways are simplified.

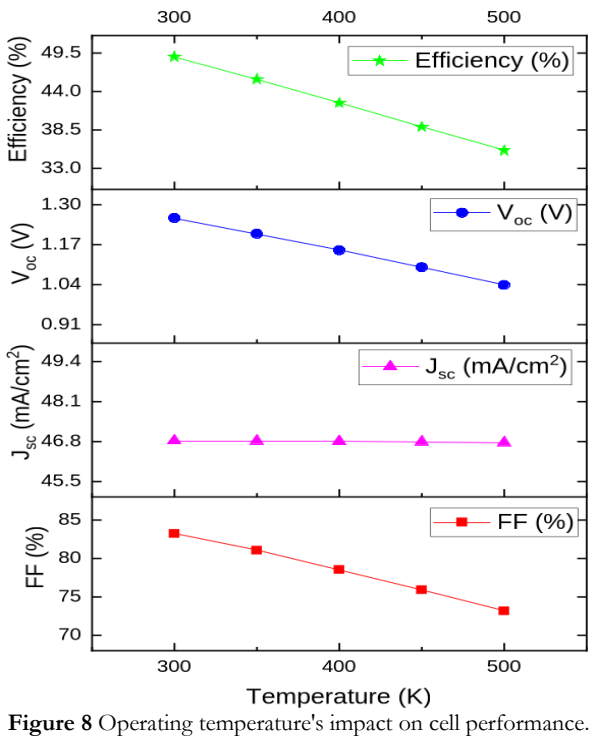

Figure 8 Operating temperature's impact on cell performance.

3.8 J-V Curve Analysis

A solar cell's performance is graphically represented by a JV (current density-voltage) curve. It gives important details regarding the cell's efficiency, fill factor, open-circuit voltage, and short-circuit current density by plotting the current density (J) versus the voltage (V).
Figure 9 shows the J-V curve characteristics for the proposed cell structure. It can be seen from curve that with BSF, the proposed cell structure showing better performance than without BSF.

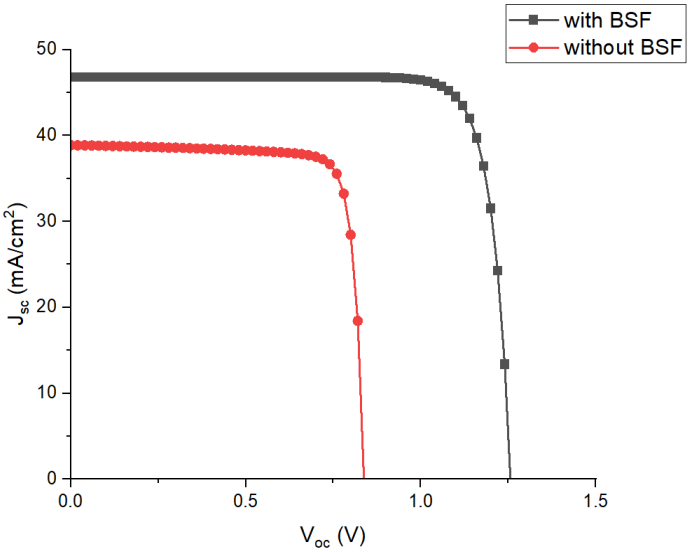

Figure 9 Comparative study of J-V characteristics curve

3.9 Quantum Efficiency of $CuSbS_2$ solar cell

The capacity of a solar cell to convert photons of different wavelengths into electrical current is measured by its quantum effectiveness, or QE. The QE spectrum of a $CuSbS_2$ solar cell shows the percentage of photons that are absorbed and changed into charge carriers (electrons or holes) as a function of wavelength.

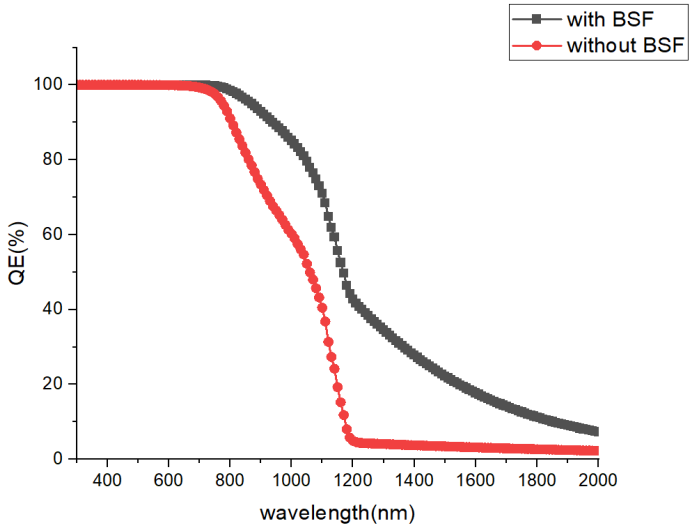

Figure 10 Quantum Efficiency of $CuSbS_2$ solar cell.

Figure 10 shows that the quantum efficiency is high at wavelengths below approximately 800 nm, where photon absorption and carrier collection are strong. The curve also shows a simulated long-wavelength response beyond 1200 nm for the dual-heterojunction structure. In the revised manuscript, this response

is not presented as conclusive evidence of real photon up-conversion. SCAPS-1D does not by itself demonstrate a physical two-step up-conversion mechanism unless such a mechanism is explicitly defined through validated energy levels, defect distributions, optical absorption coefficients, and transition processes. Therefore, the extended QE response should be interpreted as a model-dependent outcome associated with the assumed BMO optical/defect parameters and rear-junction configuration. This limitation is important because the extended QE response directly affects the high simulated Jsc and PCE values.

Table 3 Performance measurements for the cell with and without BSF

Cell Structure	Voc (V)	Jsc (mA/cm^2)	FF (%)	PCE (%)	Cell Structure
n-ZnSe/p-$CuSbS_2$	0.739	44.344	85.23	27.95	Single
n-ZnSe/p-$CuSbS_2$/p+-BMO	1.257	46.819	83.21	48.96	Dual Heterojunction

3.10 Physical interpretation and modeling limitations of the high simulated performance

The optimized n-ZnSe/p-$CuSbS_2$/p+-BMO structure gives a high simulated PCE of 48.96% with Jsc = 46.819 mA/cm^2. This value is unusually high for a $CuSbS_2$-based thin-film solar cell and is therefore treated as an idealized upper-bound result under the selected SCAPS-1D assumptions. The high current density is mainly linked to the modeled rear BMO layer and the extended simulated quantum-efficiency response. However, the present model does not provide a complete experimentally validated photon up-conversion mechanism. A rigorous demonstration would require an explicit energy-level diagram, transition pathways, governing equations, calibrated absorption coefficients, and defect/tail-state parameters. In addition, the omission of radiative recombination may artificially increase the simulated output. Consequently, the proposed structure should be understood as a promising numerical design concept that requires future validation using experimentally measured material parameters, full optical modeling, radiative and Auger recombination, and device fabrication.

4. Conclusions

ZnSe window layers and three different BSF layers were used in the simulation to compare and optimize the $CuSbS_2$ solar-cell structure. The results indicate that BSF engineering can improve carrier selectivity and rear-interface behavior. Among the investigated BSF materials, BMO produced the highest simulated performance, with the optimized n-ZnSe/p-$CuSbS_2$/p+-BMO structure giving Voc = 1.257 V, Jsc = 46.819 mA/cm^2, FF = 83.21%, and PCE = 48.96%. The BMO bandgap has been reported consistently as 1.2 eV in the revised manuscript, and all final photovoltaic parameters have been harmonized across the abstract, tables, and conclusion. However, the very high PCE and Jsc are interpreted as idealized numerical upper-limit results under the adopted SCAPS-1D assumptions. The extended QE response and any tail-state-related contribution require further theoretical and experimental validation. Future work should include complete recombination modeling, calibrated optical absorption data, experimentally measured defect parameters, and fabrication-based verification of the proposed dual-heterojunction structure.

Declaration of Ethical Standards

As the authors of this study, we declare that this manuscript complies with applicable ethical standards.

Credit Authorship Contribution Statement

H. R. Alve: Conceptualization, Methodology, Software, Investigation, Data Curation, Formal Analysis, Visualization, Writing – Original Draft Preparation.
S. Azmol: Validation, Data Curation, Investigation, Writing – Review & Editing.
M. Dey : Supervision, Conceptualization, Methodology, Project Administration, Resources, Writing – Review & Editing.

Declaration of Competing Interest

The authors declare that they have no known competing financial interests or personal relationships that could have appeared to influence the work reported in this paper.

Funding / Acknowledgements

No specific funding was received for this study. The authors declare that generative AI was used only for language editing and not for scientific content generation.

Data Availability

The simulation parameters used in this study are provided in the manuscript. Additional simulation data is available from the corresponding author upon reasonable request.

References

Asafu-Adjaye, John. 2000. "The Relationship between Energy Consumption, Energy Prices and Economic Growth: Time Series Evidence from Asian Developing Countries." *Energy Economics* 22(6):615–25. doi:10.1016/S0140-9883(00)00050-5.

Bhattacharjee, Sujoy, Mehedi Hassan, N. K. Das, and Mrinmoy Dey. 2023. "Design and Optimization of Copper Antimony Sulfide Thin Film Solar Cell." *International Journal of Renewable Energy Research* 13(V32i3). doi:10.20508/ijrer.v13i3.14107.g8812.

Borse, S. V., S. D. Chavhan, and Ramphal Sharma. 2007. "Growth, Structural and Optical Properties of Cd1−xZnxS Alloy Thin Films Grown by Solution Growth Technique (SGT)." *Journal of Alloys and Compounds* 436(1–2):407–14. doi:10.1016/j.jallcom.2006.11.009.

Branković, Z., Z. Marinković Stanojević, L. Mančić, V. Vukotić, S. Bernik, and G. Branković. 2010. "Multiferroic Bismuth Manganite Prepared by Mechanochemical Synthesis." *Journal of the European Ceramic Society* 30(2):277–81. doi:10.1016/J.JEURCERAMSOC.2009.06.030.

Deng, Chenguang, Yutong He, Wenfeng Yang, Han Yu, Zijian Hong, Hao Liu, Haojie Han, Wei Li, Yunpeng Ma, Zhongshan Zhang, Yongjun Wu, Jing Ma, Bing Xiong, Changzheng Sun, Rong Yu, Jing Feng Li, Ji Zhou, Yi Luo, and Qian Li. 2026. "Self-Buffered Epitaxy of Barium Titanate on Oxide Insulators Enables High-Performance Electro-Optic Modulators." *Light: Science and Applications* 15(1). doi:10.1038/s41377-025-02081-9.

Ferekides, C. S., D. Marinskiy, V. Viswanathan, B. Tetali, V. Palekis, P. Selvaraj, and D. L. Morel. 2000. "High Efficiency CSS CdTe Solar Cells." *Thin Solid Films* 361–362:520–26. doi:10.1016/S0040-6090(99)00824-X.

Hafizur Rahman Alve, Mrinmoy Dey, Md Hasibur Rahman, and Md Emdadul Ahsan. 2024. "Design and Optimization of Copper Zinc Tin Sulfide (CZTS) Thin Film Solar Cell." *International Journal of Smart Grid* (V8i3). doi:10.20508/ijsmartgrid.v8i3.349.g358.

Hafizur Rahman Alve, Saiful Islam, Mrinmoy Dey, and Nipu Kumar Das. 2024. "Enhancement of Power Conversion Efficiency CuSbSe2 Based Thin Film Solar Cell." *International Journal of Smart Grid* (V8i3). doi:10.20508/ijsmartgrid.v8i3.352.g362.

Islam Sakib, Md. Asiful, Md. Tamzid Ahmed, and Jitu Prakash Dhar. 2023. "Ferroelectric BiMnO3 in BSF Layer and Zinc Doped CdS in Buffer Layer: Boosting up the Performance of CZTS Solar Cell." Pp. 1–6 in *2023 International Conference on Electrical, Computer and Communication Engineering (ECCE)*. IEEE.

Javed, Farrukh. 2022. *Impact of Temperature & Illumination for Improvement in Photovoltaic System Efficiency*. Vol. 6. doi:https://doi.org/10.20508/ijsmartgrid.v6i1.222.g234.

Koroneos, Christopher, Thomas Spachos, and Nikolaos Moussiopoulos. 2003. "Exergy Analysis of Renewable Energy Sources." *Renewable Energy* 28(2):295–310. doi:10.1016/S0960-1481(01)00125-2.

Kumar, Rahul, Deepash Shekhar Saini, and Ankur Soam. 2025. "Reduced Graphene Oxide Modified with Bismuth Iron Oxide Nanoparticles for Supercapacitor Application." *Discover Applied Sciences* 7(11). doi:10.1007/s42452-025-07887-1.

Mahmood, Waqar, and Nazar Abbas Shah. 2012. "Study of Cadmium Sulfide Thin Films as a Window Layers." Pp. 178–82 in.

Martí, A., and A. Luque. 2015. "Three-Terminal Heterojunction Bipolar Transistor Solar Cell for High-Efficiency Photovoltaic Conversion." *Nature Communications* 6(1):6902. doi:10.1038/ncomms7902.

Rodriguez-Lazcano, Y., M. T. S. Nair, and P. K. Nair. 2001. *Cu x Sb y S z THIN FILMS PRODUCED BY*

ANNEALING CHEMICALLY DEPOSITED Sb 2 S 3-CuS THIN FILMS. Vol. 15. www.worldscientific.com.

Saha, Bipin, Bipanko Kumar Mondal, Shaikh Khaled Mostaque, Mainul Hossain, and Jaker Hossain. 2023. "Numerical Modeling of CuSbSe2-Based Dual-Heterojunction Thin Film Solar Cell with CGS Back Surface Layer." *AIP Advances* 13(2). doi:10.1063/5.0133889.

Sayeed, Md. Abu, and Hasan Khaled Rouf. 2019. "Numerical Simulation of Thin Film Solar Cell Using SCAPS-1D: ZnSe as Window Layer." Pp. 1–5 in *2019 22nd International Conference on Computer and Information Technology (ICCIT)*. IEEE.

Zhou, Jian, Guo-Qing Bian, Qin-Yu Zhu, Yong Zhang, Chun-Ying Li, and Jie Dai. 2009. "Solvothermal Crystal Growth of CuSbQ2 (Q=S, Se) and the Correlation between Macroscopic Morphology and Microscopic Structure." *Journal of Solid State Chemistry* 182(2):259–64. doi:10.1016/j.jssc.2008.10.025.